European Journal of Pharmaceutical Sciences 102 (2017) 24–34

Contents lists available at ScienceDirect

European Journal of Pharmaceutical Sciences

journal homepage: www.elsevier.com/locate/ejps

Improved antitumor activity and reduced toxicity of doxorubicin encapsulated in poly(ε-caprolactone) nanoparticles in lung and breast cancer treatment: An *in vitro* and *in vivo* study

Laura Cabeza [a,b,c,1], Raul Ortiz [a,d,1], Jose Prados [a,b,c,*], Ángel V. Delgado [e], Maria J. Martín-Villena [f], Beatriz Clares [d,f], Gloria Perazzoli [a,b], Jose M. Entrena [g], Consolación Melguizo [a,b,c,2], Jose L. Arias [a,b,f,2]

[a] Institute of Biopathology and Regenerative Medicine (IBIMER), Biomedical Research Centre (CIBM), University of Granada, 18100 Granada, Spain
[b] Biosanitary Institute of Granada (ibs.GRANADA), SAS-Universidad de Granada, Granada, Spain
[c] Department of Anatomy and Embryology, University of Granada, 18016 Granada, Spain
[d] Department of Health Science, University of Jaén, 23071 Jaén, Spain
[e] Department of Applied Physics, University of Granada, 18071 Granada, Spain
[f] Department of Pharmacy and Pharmaceutical Technology, University of Granada, 18071 Granada, Spain
[g] Department of Pharmacology, Institute of Neuroscience, Biomedical Research Center (CIBM), University of Granada, 18100 Granada, Spain

ARTICLE INFO

Article history:
Received 25 November 2016
Received in revised form 31 January 2017
Accepted 15 February 2017
Available online 17 February 2017

Keywords:
Doxorubicin
Poly(ε-caprolactone) nanoparticles
Lung cancer
Breast cancer
Mice xenografts
Toxicity

ABSTRACT

Poly(ε-caprolactone) (PCL) nanoparticles (NPs) offer many possibilities for drug transport because of their good physicochemical properties and biocompatibility. Doxorubicin-loaded PCL NPs have been synthesized to try to reduce the toxicity of doxorubicin (DOX) for healthy tissues and enhance its antitumor effect in two tumor models, breast and lung cancer, which have a high incidence in the global population. PCL NPs were synthesized using a modified nanoprecipitation solvent evaporation method. The *in vitro* toxicity of PCL NPs was evaluated in breast and lung cancer cell lines from both humans and mice, as was the inhibition of cell proliferation and cell uptake of DOX-loaded PCL NPs compared to free DOX. Breast and lung cancer xenografts were used to study the *in vivo* antitumor effect of DOX-loaded NPs. Moreover, healthy mice were used for *in vivo* toxicity studies including weight loss, blood toxicity and tissue damage. The results showed good biocompatibility of PCL NPs *in vitro*, as well as a significant increase in the cytotoxicity and cell uptake of the drug-loaded in PCL NPs, which induced almost a 98% decrease of the IC50 (E0771 breast cancer cells). Likewise, DOX-loaded PCL NPs led to a greater reduction in tumor volume (≈36%) in studies with C57BL/6 mice compared to free DOX in both lung and breast tumor xenograft models. Nevertheless, no differences were found in terms of mouse weight. Only in the lung cancer model were significant differences in mice survival observed. In addition, DOX-loaded PCL NPs were able to reduce myocardial and blood toxicity in mice compared to free DOX. Our results showed that DOX-loaded PCL NPs were biocompatible, enhanced the antitumor effect of DOX and reduced its toxicity, suggesting that they may have an important potential application in lung and breast cancer treatments.

1. Introduction

Doxorubicin (DOX), an anthracycline antibiotic with antineoplastic effect, is used to treat many types of solid tumors and hematological diseases such as breast, lung and ovary cancers, sarcomas, leukemia, and Hodgkin's disease (Weiss, 1992). Doxorubicin is a DNA intercalating agent that causes DNA damage resulting in cell death. In addition, this drug increases the production of reactive oxygen species (ROS) in mitochondria (Doroshow, 1983; Govender et al., 2014; Tacar et al., 2013) and interacts with the enzyme topoisomerase 2 (Top2α), which is overexpressed in cells with a high proliferation rate, such as tumor cells (Vejpongsa and Yeh, 2014). Despite DOX having an important antitumor effect, its lack of specificity for the tumor tissue makes its use limited. In fact, one of the major limitations of this drug is the production of cardiotoxicity caused by mechanisms such as ROS production (Angsutararux et al., 2015). For these reasons, it is important to develop new drug administration pathways to enhance the antitumor effect and improve specificity for tumor tissues.

Nanoparticles (NPs) of poly(ε-caprolactone) (PCL) have been investigated as antitumor drug transport and delivery systems because of their size, biocompatibility, biodegradability and the possibility of

* Corresponding author at: Institute of Biopathology and Regenerative Medicine (IBIMER), Department of Anatomy and Embryology, School of Medicine, University of Granada, 18100 Granada, Spain.
E-mail address: jcprados@ugr.es (J. Prados).
[1] These authors contributed equality to this work.
[2] CM and JLA also contributed equally to this work.

http://dx.doi.org/10.1016/j.ejps.2017.02.026
0928-0987/

modifying their surface properties increasing their multi-functionality (Dash and Konkimalla, 2012; Wei et al., 2009). In fact, many types of PCL-nanoformulations have been generated (micelles, hydrogels, scaffolds, fibers, films, and microspheres) (Dash and Konkimalla, 2012) loading numerous antitumor drugs with excellent results in both *in vitro* and *in vivo* cancer models (Liu et al., 2012). Recently, the capacity of PCL NPs to improve the antitumoral effect of classical drugs such us 5-fluorouracil, carboplatin or curcumin in colon cancer, glioblastoma and glioma, respectively, has been demonstrated (Karanam et al., 2015; Marslin et al., 2016; Ortiz et al., 2015). Concretely, DOX-loaded PCL and poly(ethylene glycol) (PEG) NPs and micelles showed a sustained drug release and great *in vitro* and *in vivo* antitumor activity compared to the free drug (Gou et al., 2009; Zhang et al., 2011). Moreover, micelles of monomethoxy PEG-PCL loaded with DOX showed better cell uptake in the B16-F10 melanoma cell line in comparison to free DOX, as well as a greater suppression of tumor growth and survival of C57BL/6 mice bearing subcutaneous melanoma tumors (Zheng et al., 2011). In addition, as demonstrated by Cheng et al. (2012), PCL micelles were able to improve DOX release in response to a temperature increase (40 °C), increasing drug cytotoxicity. Doxorubicin loaded to copolymers of dextran-β-PCL exhibited greater cytotoxicity (~15%) compared to free DOX in SH-SY5Y human neuroblastoma cell lines and a significant increase of cell internalization (Li et al., 2013). PCL and poly(*N*-vinylpyrrolidone) (PNVP) (PCL_{63}-*b*-$PNVP_{90}$) micelles loading DOX have recently been developed that enhanced growth inhibition in normal and resistant lymphoma cell lines from humans and mice in comparison with the free drug. Furthermore, these DOX-loaded nanocarriers did not alter the viability of normal blood cells such as monocytes, dendritic cells or lymphocytes (93.26%), in contrast to treatment with free DOX (60.87%) (Hira et al., 2014). Latterly, polymers containing PCL have been developed to release the drug under certain conditions to make it even more specific to the tumor tissue, such as photocleavable polymers, or involving the incorporation of cleavable disulfide linkages by the intracellular enzyme glutathione (Kumar et al., 2015; Lee et al., 2015).

In this context, the aim of our study was to use a formulation of PCL NPs for transporting DOX in order to potentially improve breast and lung cancer treatment. Cell proliferation assays with breast and lung cancer cell lines from both humans and mice, and cellular internalization studies using FACScan and fluorescent microscopy were performed. In addition, *in vivo* studies were carried out to look at the antitumor effect of DOX-loaded PCL NPs compared to free DOX, mice survival, and modulation of DOX toxicity. The results showed good biocompatibility of PCL NPs and a significant increase in DOX antitumor effect when drug was loaded to PCL NPs. No differences were found in the weight of mice when the free DOX and DOX-loaded PCL NP treatments were compared. Interestingly, a modulation of mice survival was observed with the use of DOX-loaded NPs. Finally, decreased DOX toxicity on blood and tissue was determined. Thus, the use of DOX-loaded PCL NPs improves the drug's antitumor effect, something which could be applied in the treatment of breast and lung cancer.

2. Material and methods

2.1. Materials

All chemicals were of analytical quality from Sigma-Aldrich Chemical Co. (Spain). Deionized and filtered water was used in all the experiments (Milli-Q Academic, Millipore, Molsheim, France).

2.2. Formulation of DOX-loaded PCL NPs

PCL NPs were prepared by a modified nanoprecipitation solvent evaporation procedure using a probe sonicator (Branson sonifier W450 Digital, Branson Ultrasonics, Danbury, CT, USA) (Cirpanli et al., 2011; Letchford et al., 2009). Concretely, 1 mL of a dichloromethane (DCM) polymeric solution (1%, w/v) was added drop-wise, under sonication (pulsed mode, with a cycle of 70%, to avoid foaming), to 5 mL of an aqueous solution containing Pluronic® F-68 (0.3%, w/v). Temperature control was assured by surrounding the sample vial with ice during the sonication process (1 h). Finally, the organic solvent was evaporated (Büchi Rotavapor® rotary evaporator, Büchi, Flawil, Switzerland), and the colloid was subjected to a cleaning process involving subsequent cycles of centrifugation (30 min at 9000 rpm, Centrikon T-124 high-speed centrifuge; Kontron, Paris, France) and re-dispersion in water, until the conductivity of the supernatant was <10 μS/cm.

DOX entrapment into PCL NPs was based on the above described formulation methodology with an additional step aiming to optimize the drug loading efficacy: incorporation of a DCM polymeric solution containing adequate quantities of DOX (up to 0.01 M) to the aqueous medium, or addition of the DCM polymeric solution to the aqueous phase containing increasing drug concentrations (up to 10^{-2} M). The objective was to clarify if greater drug entrapment (and loading) efficacies are possible when DOX molecules are included in direct contact with the polymer (dissolved in the organic phase to minimize drug escape to the aqueous phase). Additionally, the impact on DOX entrapment of the concentration of stabilizing agent (Pluronic® F-68) and polymer (PCL) was analyzed. To that aim, the concentration of PCL in the DCM solution and the concentration of Pluronic® F-68 in the aqueous medium were varied from 1 to 5% (w/v) and from 0 to 5% (w/v), respectively. All the formulations were prepared in sextuplicate.

2.3. Characterization methods

Particle size (mean value ± standard deviation) was determined in quadruplicate at room temperature by photon correlation spectroscopy (PCS, Malvern Autosizer® 4700, Malvern Instruments Ltd., UK), after suitable dilution of the aqueous NP dispersions (≈0.1%, w/v). Stability of the colloids was investigated during three months of storage at 4.0 ± 0.5 °C in water by measuring both the size and DOX loading. Finally, to confirm the size analysis, aqueous NP dispersions (≈0.1%, w/v) were visualized by high resolution transmission electron microscopy (HRTEM, Stem Philips CM20 high resolution transmission electron microscope, Netherlands).

Surface electrical charge of both blank (DOX unloaded) and DOX-loaded NPs was investigated by electrokinetic determinations (≈0.1%, w/v NP concentration in aqueous media) (Malvern Zetasizer® 2000 electrophoresis device, Malvern Instruments Ltd., UK), after 24 h of contact of NPs in water (pH ≈ 6) under mechanical stirring (50 rpm) at room temperature. Such electrophoretic characterization was expected to define the type of drug loading (adsorption onto the NP surface, or entrapment into the nanomatrix).

Ultraviolet-Visible (UV–Vis) absorbance measurements (8500 UV–Vis Dinko spectrophotometer, Dinko, Spain) were done in quadruplicate at the maximum absorbance wavelength (481 nm) to quantify drug concentration in all the formulations. Before determining the amount of DOX loaded to (or released from) the PCL NPs, the UV–Vis spectrophotometric method of analysis was validated (and verified) by comparing the evaluation of drug concentration in 2 instances: a certain DOX quantity was dissolved in supernatants of NP syntheses (done in absence of drug), and the same amount was dissolved in equal amounts of water. Drug concentrations estimated (in the first case from the difference between the absorbance of DOX plus supernatant solution and that of the supernatant) were found to match within the experimental uncertainty. These tests were done in sextuplicate, and demonstrated the accuracy, precision, and linearity of the method, and the absence of molecular interactions.

DOX loading studies involved UV–Vis determinations of the drug remaining in the aqueous supernatant (being obtained upon centrifugation, 30 min at 9000 rpm, of the NP dispersion) which was deduced from the total amount of DOX in the aqueous NP dispersion. For the method to be accurate, the contribution to the absorbance of sources

other than variations in drug concentration (*e.g.* Pluronic® F-68), by subtracting the absorbance of the supernatant produced in the same conditions but without the drug. DOX incorporation to the NPs was expressed in terms of drug loading (%) and drug entrapment efficiency (%):

$$\text{Drug loading}\,(\%) = \frac{\text{mass of drug incorporated in the NP matrix}\,(\text{mg})}{\text{mass obtained of NPs loaded with drug}\,(\text{mg})} \times 100$$

$$\text{Drug entrapment efficiency}\,(\%) = \frac{\text{mass of drug incorporated in the NP matrix}\,(\text{mg})}{\text{mass of drug used in the experiment}\,(\text{mg})} \times 100$$

Drug release experiments were performed in quadruplicate following the dialysis bag method, and using the nanoformulations that were investigated later *in vitro* and *in vivo* (PCL NPs with the greater DOX loading values, *i.e.* ≈49%, Table 1). The bags were soaked in water at room temperature during 12 h before use. The dialysis bag (cut-off of 2000 Da, Spectrum® Spectra/Por® 6 dialysis membrane tubing, USA) retained the particles but permitted the free drug to diffuse into the receiving phase (phosphate buffered saline, PBS, pH 7.4 ± 0.1, kept at 37.0 ± 0.5 °C). Then, 1 mL of NP dispersion (containing 4 mg/mL of DOX) was poured into the dialysis bag with the two ends fixed by clamps. The bag was then placed in a conical flask filled with 50 mL of PBS, and was stirred at 150 rpm. At different time intervals (0.5, 1, 3, 6, 9, 12, 24, 48, 72, 96, 120, and 144 h), 1 mL samples of the medium were withdrawn for UV–Vis spectrophotometric analysis (481 nm). An equal volume of the release medium, kept at the same temperature, was added after sampling to ensure the sink conditions.

2.4. Cell culture

The human cell lines MCF-7 and A549 of breast and lung cancer respectively, were obtained from the European Collection of Cell Culture and the Scientific Instrumentation Center (University of Granada, Spain). The LL/2 mouse lung cancer cell line, were purchased from the American Type Culture Collection (ATCC), and the E0771 mouse breast cancer cell line were kindly given by Robin Anderson from Peter MacCallum Cancer Center, (East Melbourne, Australia). Both mouse cell lines come from the immunocompetent mouse C57BL/6. In addition, a rat cardiomyocyte cell line (H9C2) obtained from ATCC was used for toxicity assays. All cell lines were grown in monolayer in Dulbecco's Modified Eagle's Medium (DMEM) (Sigma-Aldrich) with a supplementation of 10% fetal bovine serum (FBS) and 1% of antibiotics (Penicillin-Streptomycin) (Sigma-Aldrich) and maintained at 37 °C in a humidified incubator with an atmosphere of 5% CO_2.

2.5. In vitro cytotoxicity of cell lines

Cell proliferation was determined by a modified sulforhodamine B (SRB) assay as described previously (Melguizo et al., 2015). All the experiments were performed in triplicate. Cells lines were plated in 24-well plates at different cell densities: 10×10^3, 15×10^3, 20×10^3, 15×10^3 cells/well for MCF-7, A549, LL/2 and E0771, respectively. In addition, the non-tumor H9C2 rat embryonic cardiomyocyte cell line was plated at a density of 8×10^3 cells/well. Twenty-four hours later, cells were treated with DOX, DOX-loaded PCL NPs and unloaded PCL NPs at concentrations ranged from 0.01 to 10 μM at an incubation time of 48 h. The concentration of unloaded PCL NPs used was equivalent to the drug-loaded NPs. Untreated cells were used as a negative control. After the incubation time, cells were fixed with 10% trichloroacetic acid (TCA), stained with SRB, and the dye was resuspended with a 10 mM, pH 10.5 solution of Trizma and quantified at 492 nm with a Titertek Multiskan™ colorimeter (Flow Laboratories, Irvine, UK). The optical density (OD) of treated cells was compared with the OD of untreated cells (100% of viability) to determine the percentage of relative inhibition (%IR) produced by the treatments.

2.6. Flow cytometry assay

To study the rate of incorporation of drug-loaded to NPs compared to free drug, we subjected the cells to a flow cytometry (FACScan) assay. All the cell lines were plated in 6-well plates at a cell density of 150×10^3 cells/well in 2 mL of DMEM. After 24 h, treatments at 25 μg/mL of DOX and DOX-PCl NPs were added to cells and incubated at 0.5, 1, 1.5, 2, and 4 h. After the incubation time, cells were detached by trypsinization, and the cell pellets were collected by centrifugation at 1500 rpm for 5 min and resuspended in 200 μL of PBS solution. Flow cytometry analysis was carried out with a FACSCanto II flow cytometer (BD Bioscience, San Diego, CA, USA).

Table 1
Influence of the preparation conditions (DOX, PCL, and Pluronic® F-68 concentrations) for drug absorption on particle size, drug entrapment efficiency (%), drug loading (%), and zeta potential (ζ, mV) values of the blank (DOX unloaded) PCL NPs and the DOX-loaded PCL NPs formulated after drug dissolution in the organic phase. Size, entrapment efficiency, drug loading, and ζ values of DOX-loaded PCL NPs obtained after drug dissolution in the aqueous media are given inside curve brackets.

[DOX] (M)	[PCL] (%, w/v)	[Pluronic® F-68] (%, w/v)	Size (nm)	DOX entrapment efficiency (%)	DOX loading (%)	ζ (mV)
0	1	0.3	73 ± 13	–	–	−14 ± 3
10^{-5}	1	0.3	77 ± 9 (79 ± 8)	36.4 ± 2.3 (26.1 ± 3.4)	0.019 ± 0.005 (0.014 ± 0.006)	−15 ± 1 (−16 ± 3)
10^{-4}	1	0.3	79 ± 6 (80 ± 7)	60.7 ± 3.7 (37.3 ± 3.1)	0.329 ± 0.063 (0.203 ± 0.044)	−15 ± 1 (−16 ± 3)
10^{-3}	1	0.3	70 ± 8 (73 ± 8)	82.1 ± 4.1 (53.3 ± 3.2)	4.462 ± 0.121 (2.908 ± 0.096)	−17 ± 2 (−14 ± 1)
10^{-2}	1	0.3	83 ± 7 (69 ± 8)	90.6 ± 3.6 (59.8 ± 4.1)	49.242 ± 3.091 (32.502 ± 3.976)	−15 ± 2 (−15 ± 3)
10^{-2}	1	0	Macroaggregates	–	–	–
10^{-2}	1	1	77 ± 9 (85 ± 4)	92.6 ± 4.1 (60.5 ± 3.8)	50.226 ± 3.578 (32.859 ± 3.321)	−16 ± 4 (−17 ± 3)
10^{-2}	1	3	67 ± 5 (87 ± 2)	86.1 ± 3.3 (55.2 ± 4.4)	46.796 ± 3.014 (30.002 ± 4.112)	−14 ± 3 (−15 ± 1)
10^{-2}	1	5	77 ± 8 (74 ± 6)	88.3 ± 4.2 (58.1 ± 3.3)	47.992 ± 3.629 (31.578 ± 3.016)	−14 ± 4 (−13 ± 4)
10^{-2}	3	0.3	75 ± 6 (73 ± 6)	89.8 ± 3.2 (58.7 ± 3.6)	16.269 ± 1.227 (10.635 ± 1.674)	−15 ± 1 (−13 ± 3)
10^{-2}	5	0.3	80 ± 9 (77 ± 6)	93.6 ± 2.9 (62.4 ± 1.5)	10.175 ± 1.016 (6.783 ± 0.962)	−16 ± 2 (−15 ± 3)

2.7. Fluorescent microscopy assay

All cell lines were seeded in a volume of 300 μL in chamber slides (BD Biosciences, Erembodegem, Belgium) of 8 wells at a cell density of 5×10^3 cells/well. After 24 h in culture conditions, cells were exposed to the same dose of free DOX and DOX-loaded PLC NPs as in the cytometry assay (25 μg/mL) at 45 min of incubation. After the incubation time, 200 μL of 4% formaldehyde was added to cells for 20 min at room temperature. Then, cells were washed three times with PBS and the cell nuclei were stained with 4′,6-diamidino-2-phenylindole (DAPI, Invitrogen ™). Drug intracellular location was observed under fluorescence microscopy using a Leica DM IL LED fluorescence microscope (Leica Microsystems S.L.U., Barcelona, Spain).

2.8. In vivo antitumoral activity of the DOX-loaded PCL NPs

Two groups of forty female C57BL/6 mice (Charles River, Barcelona, Spain) were s.c. inoculated in the right hind flank with a half million of LL/2 or E0771 cells in a volume of 200 μL of phosphate buffered saline (PBS) to induce s.c. lung and breast tumors, respectively. After nine days, each group of mice bearing tumors was divided randomly into groups of ten mice, and each was treated i.v. with DOX (10 mg/kg), DOX-loaded PCL NPs (with the equivalent drug concentration) and blank PCL NPs. Besides, there was one group of each type of cancer treated with saline solution as a negative control. The treatments were applied every three days for a total of five doses. Furthermore, every three days the weight of mice were monitorized and also the tumor dimensions were measured with a digital caliper, and the tumor volume was calculated with the formula $V(mm^3) = (a \times b^2 \times \pi)/6$, (being "a" the largest diameter of the tumor, and "b" the largest diameter perpendicular to "a"). The final point of the experiment when animals were sacrificed was the day 33 starting from the day of cells inoculation. The animal studies were approved by the Ethics Committee on Animal Experimentation of the University of Granada.

2.9. In vivo toxicity study of DOX-loaded PCL NPs

To determine the *in vivo* toxicity of DOX-loaded NPs, 32 female C57BL/6 mice were divided randomly into four groups ($n = 8$). Following the protocol of Zhu et al. (2015), single doses of DOX (10 mg/kg body) and DOX-loaded NPs (with the equivalent drug concentration) were injected i.v. into healthy mice. A group treated with blank PCL NPs and another untreated group (control) were also included in the study. Mouse body weight was determined every 48 h until the final point of the experiment (14 days from the treatment). Tissue (heart, liver and lung) and blood samples were obtained on the fourth day after treatments. Tissues from 3 mice of each group were fixed in a 4% paraformaldehyde (PFA) solution, embedded in paraffin, sectioned (5 μm) and finally stained with hematoxylin and eosin. The samples were observed in a Leica DM IL LED microscope (Leica Microsystems S.L.U., Barcelona, Spain). Blood was extracted from all the mice in 1.5 mL EDTA-coated Eppendorf tubes for the analysis of blood parameters (Mythic 22CT C2 Hematology Analyzer, Orphée SA, Switzerland). A portion of blood was gently mixed and centrifuged (15 min at 3.000 rpm a 4 °C) to obtain plasma which was then aspirated from the collection tubes and stored at −80 °C. Three cardiovascular disease markers, MMP-9 (Matrix metallopeptidase 9), sVACM-1 (vascular cell adhesion molecule-1) and CRP (C-reactive protein) were evaluated using Milliplex MAP Kits (Merck Millipore; Darmstadt, Germany). Optical density was determined using an automated immunoassay analyzer, the Luminex 200 TM (Millipore, Darmstadt, Germany).

2.10. Statistical analysis

All the results have been expressed as the mean ± the standard deviation. Statistical analysis of the *in vitro* studies was carried out with the Student's *t*-test. For the *in vivo* studies, a one-way ANOVA with a Tukey's *post-hoc* test was used to evaluate the differences between groups in terms of tumor volume and toxicity. Mice survival *P* was calculated with the Kaplan-Meier method and then analyzed with the log-rank test. All the tests were performed with the Statistical Package for the Social Sciences (SPSS) v. 15.0 with a significance level of 0.05 ($\alpha = 0.05$).

3. Results

3.1. Characterization of the DOX-loaded PLC NPs

PCL NPs obtained using a modified nanoprecipitation solvent evaporation procedure were characterized by having an average diameter of <90 nm and a spherical shape (Table 1, Fig. 1). The negative surface electrical charge of the NPs in water (Table 1) could be attributed to the dissociation, at pH 6, of free acrylic groups included in their chemical structure (Arias et al., 2010). No differences were observed in particle size and quality of the colloid when the NPs were loaded with different amounts of DOX (Table 1). Finally, the colloidal formulations were found to be stable during a three-month storage period at 4.0 ± 0.5 °C: no appreciable change in particle size and surface electrical charge, no existence of aggregates/sediments, nor any DOX precipitation and/or release were detected.

Investigation of DOX entrapment in the PCL NPs began by defining the influence of the initial phase (aqueous or organic) in which the drug was dissolved (see Section 2.2, Formulation of DOX-loaded PCL NPs). DOX entrapment efficiency (%) and DOX loading values (%) as a function of the drug concentration are compiled in Table 1. Both parameters were found to be significantly greater when DOX was added to the organic phase, whatever the initially fixed drug quantity. As an example, when the initial DOX concentration was 10^{-2} M these parameters rose from ≈59.8% and ≈32.5% (when the drug was in the aqueous phase) to ≈90.6% and ≈49.2% (when DOX was incorporated to the DCM solution), respectively. This could be a consequence of the difficulty experienced by the drug in escaping from the PCL nanomatrix when it is placed in deep contact with the polymer. Finally, there may be further attractive forces between the positively-charged drug molecules and the negatively-charged NPs, thus electrostatically favoring DOX incorporation to the NPs. Antiproliferative and *in vivo* tumor growth inhibition studies were performed using the NPs with the greatest DOX entrapment efficiencies, *i.e.*, ≈90.6%.

Table 1 reveals how drug concentration positively influenced the efficiency of DOX entrapment into the NPs. It can be further highlighted that the use of Pluronic® F-68 assured homogeneous distributions of DOX-loaded NPs, highly uniform and with reduced size, without

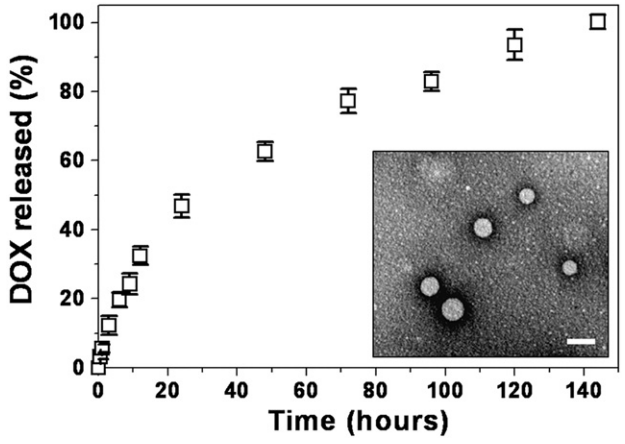

Fig. 1. DOX released (%) from PCL NPs as a function of the incubation time (h) in PBS (pH 7.4 ± 0.1) at 37.0 ± 0.5 °C. Data presented as mean value ± standard deviation (S.D.) ($n = 4$). Inset: high-resolution transmission electron microphotograph of the NPs (bar length: 100 nm).

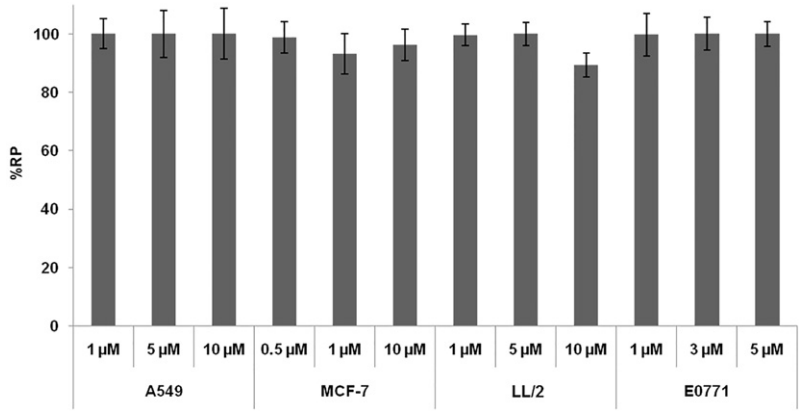

Fig. 2. *In vitro* cytotoxicity of PCL NPs in lung and breast cancer cells. The growth of cell lines A549, MCF-7, LL2 and E0771 was evaluated after exposure to a wide range (0.5–10 μM) of blank PCL NPs over a 48 h period. The results are expressed as %RP. The data represents the mean value ± S.D. of triplicate cultures.

significantly affecting DOX entrapment. Similarly, the quantity of polymer did not exhibit an important influence on DOX loading.

Great similarity was found between the electrokinetics (ζ values) of blank NPs and DOX-loaded NPs (Table 1). In fact electrophoretically speaking they were indistinguishable. Given the extraordinary sensitivity of electrophoresis to tiny changes in colloidal surfaces, this technique was advantageously used to define the type of DOX incorporation to the NPs (surface adsorption *vs.* entrapment within the nanomatrix). Due to the fact that ζ values did not change upon drug incorporation, it can be assumed that the DOX molecules were entrapped within the NP structure.

With regard to DOX release from the NPs, a biphasic process was observed at pH 7.4, characteristic of PCL nanomatrices (Pohlmann et al., 2013), where an initial rapid (burst) release phase (up to ≈30% in 12 h) was followed by a phase in which the remaining drug molecules were released in a more progressive way (over a period of 5.5 days) (Fig. 1). Thus, the majority of DOX may be located within the PCL matrix rather than adsorbed onto the particle surface.

3.2. DOX-loaded PLC NPs cell toxicity

Blank PCL NPs showed no toxicity in any of the tested cell lines even at the highest concentrations. Only a slight decrease (10%) in the percentage of relative proliferation (% RP) was detected in the LL/2 cells when blank NPs were used at 10 μM (Fig. 2). On the other hand, DOX-loaded NPs showed a significant increase in the inhibition of proliferation in all cell lines after 48 h of exposure in relation to the free drug ($p < 0.05$) (Fig. 3). This increased DOX cytotoxicity led to a significant reduction in the half-inhibitory concentration (IC50) which was 0.71, 0.7, 0.11 and 1.3 μM for DOX and 0.31, 0.09, 0.04, and 0.02 μM for DOX-PCL NPs in the A549, MCF-7, LL/2 and E0771 cell lines, respectively. The greatest decreases of the IC50 values were detected in MCF-7 (87.1%)

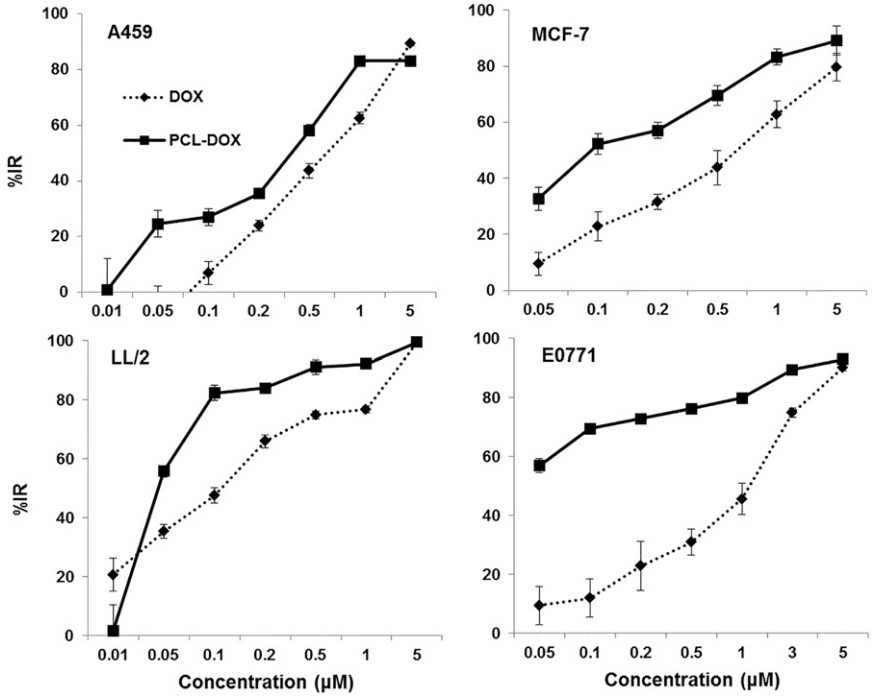

Fig. 3. *In vitro* cytotoxicity of DOX-loaded PCL NPs in lung and breast cancer cells. The growth of cell lines was evaluated after exposure to a wide range (0.01–5 μM) of DOX-loaded PCL NPs for 48 h, in comparison to free DOX treatment. The results are expressed as %IR. The data represents the mean value ± S.D. of triplicate cultures.

and E0771 (98.5%). In addition, a cytotoxic assay was performed with the non-tumor H9C2 rat embryonic cardiomyocyte cell line (Supplementary material; Fig. 1S).

3.3. DOX-loaded PLC NPs cell internalization assays

Flow cytometry analysis showed that the time-dependent internalization of DOX significantly increased in all cell lines when the drug was loaded in PCL NPs in comparison to the free drug (Fig. 4). This increase was more evident from 2 h of exposure and was maintained until 4 h. At this time, the increase in drug internalization with DOX-loaded NPs was 63.2, 35.8, 18.1 and, 33.9% in the A549, MCF-7, E0771 and LL/2 cell lines, respectively compared to the free drug. These findings were supported by fluorescence microscopy analysis (Fig. 5) where the fluorescence intensity of all human and murine cells treated with DOX-loaded PCL NPs was significantly greater that those treated with free DOX. The intracellular location of the free DOX and drug-loaded NPs was similar (predominantly nuclear), although the presence of the drug in the cytoplasm also was detected after treatment with DOX-loaded PCL NPs.

3.4. DOX-loaded PLC NPs effect in breast and lung cancer xenografts

Fig. 6 shows the results obtained in the studies realized with the immunocompetent C57BL/6 mice bearing subcutaneous lung or breast tumors. No significant differences were found between the tumor volume of mice treated with blank PLC NPs and the negative control mice treated with saline solution in either mice tumor model. Conversely, mice treated with DOX-loaded PLC NPs showed a significantly higher decrease in tumor volume than that observed in mice treated with free DOX, in both mice tumor models ($p < 0.05$). At the end point of the assay, the reduction in tumor volume in both breast and lung xenografts was similar (≈36%) (Fig. 6A). In addition, a significantly increased survival rate was detected in mice bearing lung tumors treated with DOX-PCL NPs compared with the free drug ($p < 0.05$). However, these differences were not observed in mice with breast cancer (Fig. 6B). These results are reflected in the Kaplan-Meier curves, where the fraction surviving in mice bearing breast tumors is almost the same for DOX- and DOX-loaded PCL NP-treated mice (Fig. 6B). Finally, no significant differences in mice survival were found when performing the log-rank test between control and blank PCL treated mice in both tumor models.

3.5. DOX-loaded PLC NPs in vivo toxicological study

Firstly, the weight of treated and non-treated mice was measured every three days throughout the 33 days of previous study to indicate any possible drug toxicity. As shown in Fig. 7, the negative control mice and PCL NP-treated mice showed a similar weight evolution indicating the biocompatibility and non-toxicity of the NPs. In addition, no significant differences were detected between mice treated with the free drug and drug-loaded NPs in either mice model.

Secondly, tissue and blood toxicity was evaluated. Histological analysis showed that the myocardial tissue of mice treated with free DOX showed some myofibrillar loss, a typical finding due to the cardiomyopathy induced by this drug. Interestingly, no myocardial alteration was observed in animals treated with DOX-loaded PCL NPs in comparison to the controls (Fig. 8A). Studies of other tissues (liver and lung) showed no relevant injuries, at least at this DOX concentration (Fig. 8A). In order to assess the possible myocardial injury, cardiovascular damage blood markers were analyzed. As shown in Fig. 8B, the blood level of CRP after free DOX treatment was significantly higher (49.7%) in comparison to the control ($p < 0.05$). In contrast, no significant differences between DOX-loaded PCL NP-treated mice and untreated mice (control) were detected. Additionally, no significant differences were observed between groups, for the two others blood markers (MMP-9 and sVACM-1) quantified. Moreover, during the study of toxicity (14 days), no significant differences were found in the weight of mice treated with DOX-loaded PCL NPs and free DOX (Fig. 8C). The blank PCL NPs induced no significant modifications in any of the tested tissues or blood markers, nor in weight of the mice (data not shown).

Finally, the blood analysis showed a significant decrease in the WBC value of the mice treated with free DOX. In contrast, the use of DOX-loaded PCL NPs did not modify the WBC value compared with the

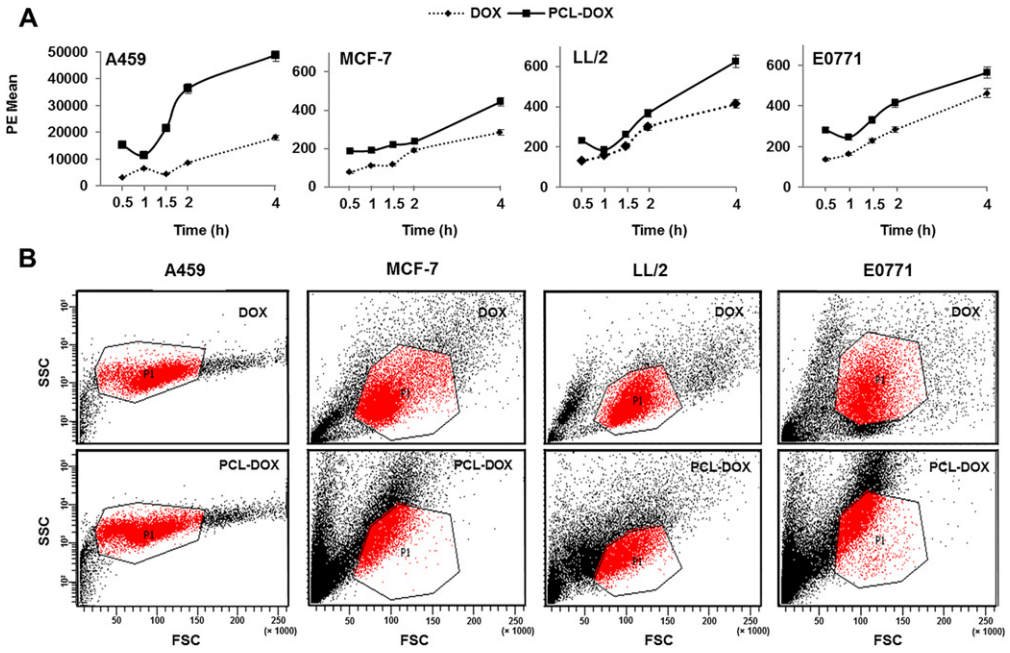

Fig. 4. Uptake of DOX-loaded PCL NPs into lung and breast cancer cells. (A) Graphical representation of the presence of DOX-loaded PCL NPs and free DOX in lung and breast cancer cells after exposure (0.5, 1, 1.5, 2 and 4 h) at 25 μg/mL drug concentration. (B) Representative image of flow cytometry analysis after exposure (4 h) to DOX-loaded PCL NPs and free DOX, in lung and breast cancer cells. The data represents the mean value ± S.D. of triplicate analysis.

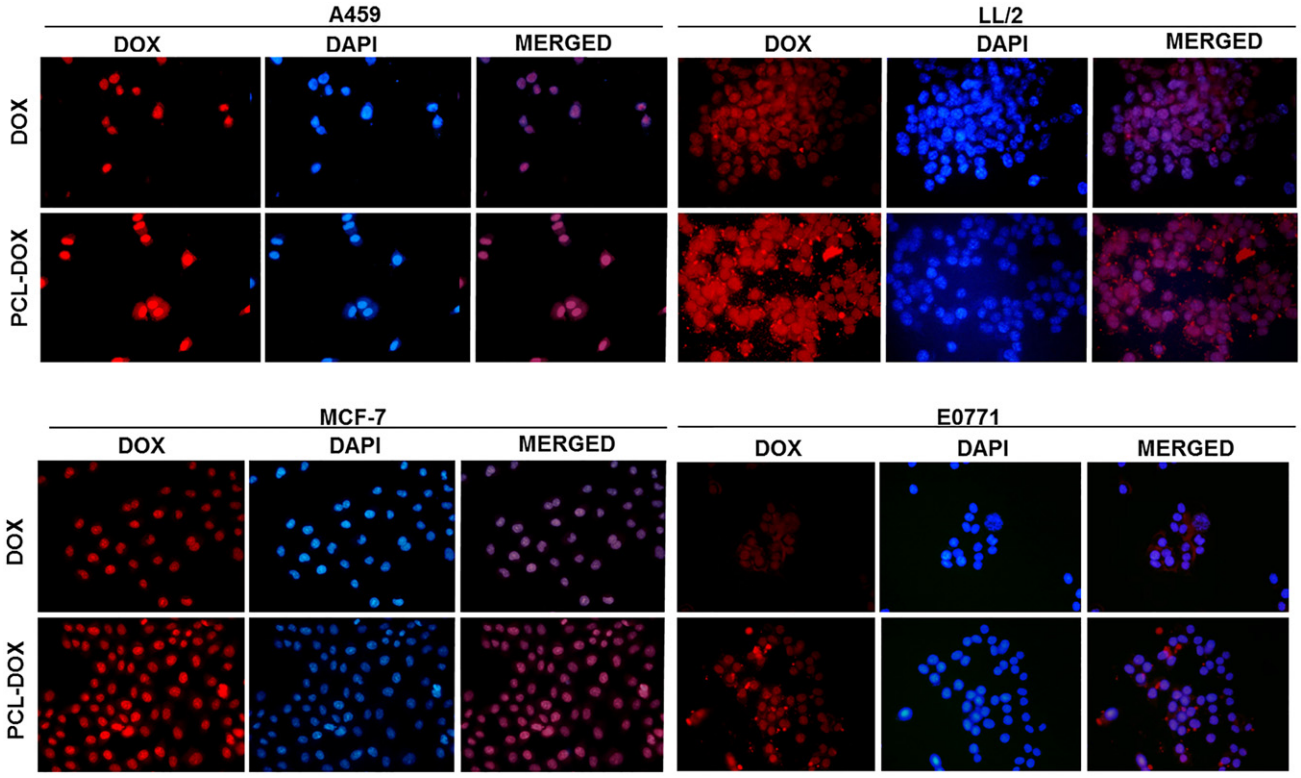

Fig. 5. Representative fluorescence images showing internalization of free DOX and DOX-loaded PCL NPs in lung and breast cancer cells after exposure to a concentration of 25 μg/mL for 45 min. The columns show drug fluorescence images (DOX), cell nuclei stained with DAPI (DAPI), and merged images of the two previous columns (MERGED). Magnification 10×.

blood used as a control. No statistically significant changes were detected in RBC or PLT values with the use of free DOX or DOX-loaded PCL NPs. A slight decrease in the MCV value was detected with the use of free DOX, DOX-loaded PCL NPs, and PCL NPs. In the same way, slight modifications were observed in MHC, MPV and RDV with the use of these different treatments (Table 2).

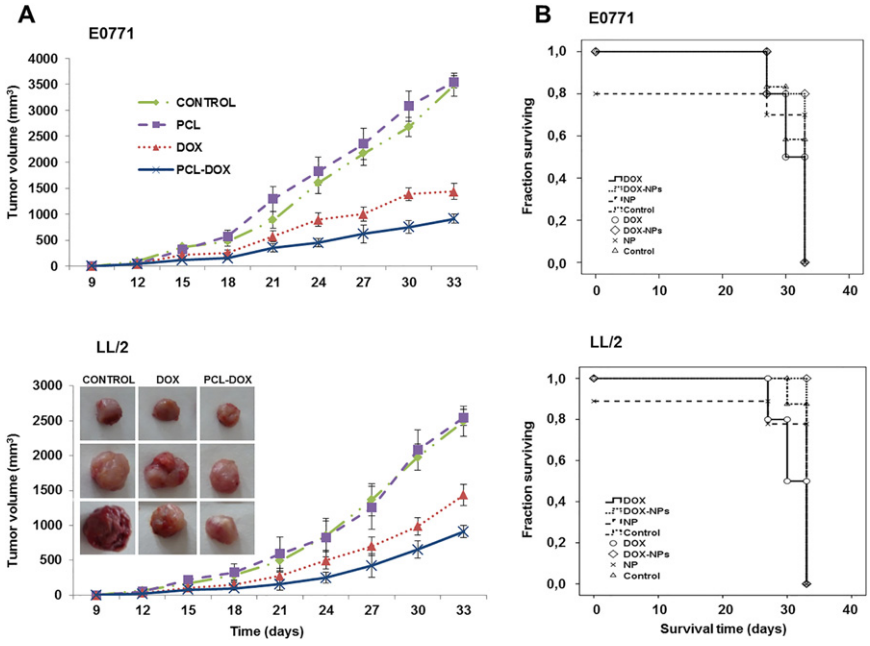

Fig. 6. Treatment of breast and lung cancer xenografts with DOX-loaded PCL NPs. (A) Graphical representation of the tumor volume progression (growth inhibition) after intravenous administration of DOX-loaded PCL NPs, free DOX and blank PCL NPs into C57BL/6 mice bearing subcutaneous tumors induced by the E0771 and LL/2 cell lines. Data are represented as the mean ± S.D. ($n = 10$). Graphical representation of LL/2 including a representative image of the tumor volume progression after treatment. (B), Kaplan-Meier curves of mice survival rates after exposure to the same treatments. Data are represented as the mean value ± S.D. ($n = 10$). Comparison between treatment groups was performed with the log-rank test.

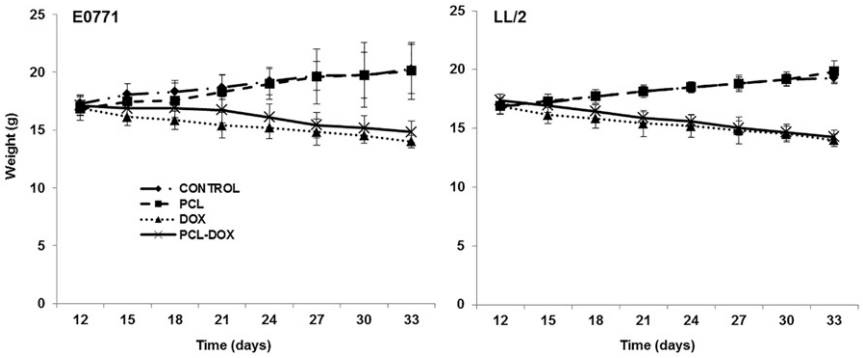

Fig. 7. Body weight progression of mice with induced lung and breast tumors after DOX-loaded PCL NP treatment. Weight of mice treated with DOX-loaded PCL NPs, free DOX, and blank PCL NPs were measured until the final point of the experiment throughout a 33-day period. The data were represented as the mean value ± S.D. ($n = 10$).

4. Discussion

Breast and lung cancer are the two types of tumors with the highest incidence worldwide. Despite the advances in chemotherapy treatment, both types of tumors result in a large numbers of deaths (Ferlay et al., 2013). The main reason for the failure of current chemotherapy is related to its lack of specificity and the induction of high levels of toxicity that result in very debilitating side effects for patients. This fact makes it necessary to limit the drug dose that then is sometimes not enough to stop the progress of the disease (Blanco and Ferrari, 2014). Our study shows the beneficial properties of DOX-loaded PCL NPs in improving the antitumoral activity of the drug against breast and lung tumors. In particular, our NPs allowed a greater DOX encapsulation and a biphasic drug release, increased cellular internalization, and also achieved a clear decrease in the DOX IC50 value *in vitro* and a decrease in tumor volume *in vivo*, supporting the potential of PCL NPs for anticancer agent delivery (Gou et al., 2011).

The synthesis of DOX-loaded PCL NPs was based on a modified nanoprecipitation solvent evaporation procedure (Cirpanli et al., 2011; Letchford et al., 2009) involving the use of a probe sonicator. This technique generated DOX-loaded NPs with an average size of <90 nm (Table 1), which could be sufficient to facilitate cellular uptake and hence produce a significant concentration of drug molecules within cancer cells (Decuzzi et al., 2009). The best preparation conditions were defined to

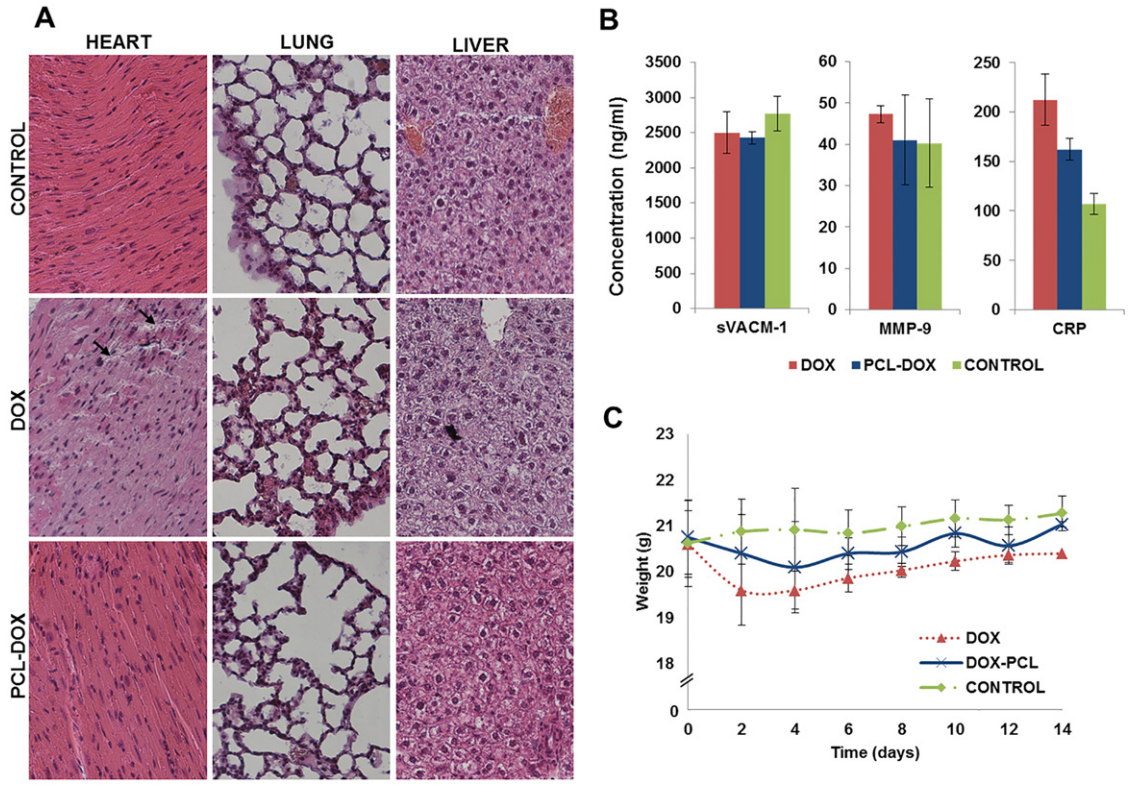

Fig. 8. *In vivo* DOX-loaded PCL NPs toxicity study in mice. C57BL/6 mice were treated with a single dose of free DOX and DOX-loaded PCL NPs (10 mg/kg). Untreated mice were the control group. (A) Tissue toxicity (heart, lung and liver) was analyzed using hematoxylin and eosin staining (Magnification 20×), revealing signs of cardiotoxicity (myofibrillar disruption) (arrows) when DOX was used. (B) Graphical representation of blood markers of cardiovascular damage showing elevated CRP levels when DOX was used. The data are represented as the mean value ± S.D. (C) Body weight progression. The weight of mice was measured every two days from the day of drug inoculation until day 14. The data are represented as the mean value ± S.D.

Table 2
Analysis of blood parameters in mice treated with DOX, PCL-DOX and PCL NPs.

Blood parameters	CONTROL	DOX	PCL-DOX	PCL
WBC (10^3/μL)	6.38 ± 1.41	3.98 ± 0.44*	6.40 ± 1.71	4.49 ± 0.80
RBC (10^6/μL)	10.27 ± 0.47	9.28 ± 1.08	9.37 ± 0.62	8.16 ± 1.85
HGB (g/dL)	16.27 ± 0.80	15.03 ± 1.70	15.03 ± 1.03	13.26 ± 2.99
HCT (%)	47.75 ± 2.41	42.07 ± 4.99	42.67 ± 2.76	37.06 ± 8.58
RDW	14.08 ± 0.56	14.35 ± 0.32	14.85 ± 0.48*	14.69 ± 0.32
PLT (10^3/μL)	634.17 ± 80.76	817.33 ± 162.57	690.83 ± 57.86	615.5 ± 224.83
PCT (%)	0.37 ± 0.04	0.47 ± 0.10	0.41 ± 0.03	0.37 ± 0.13
PDW	21.13 ± 1.12	20.08 ± 3.21	22.42 ± 2.52	22.84 ± 3.16

WBC, white blood cells; RBC, total red blood cells; HGB, hemoglobin, HCT, hematocrit; RDW, red cell distribution width; PLT, total platelets; PCT, plateletcrit; PDW, platelet distribution width. The data represents the mean value ± S.D. ($n = 8$).
* $p < 0.05$ compared to control.

be those assuring the greatest drug loading. DOX was assumed to be entrapped within the PCL matrix rather than just adsorbed onto the particle surface, given the similarities between the electrokinetics (ζ values) of blank NPs and drug-loaded NPs (Table 1). The biphasic (and sustained) DOX release profile (depicted in Fig. 1) could be the consequence of an initial fast drug release (loss of poorly entrapped DOX molecules rapidly diffusing into PBS), followed by a slower second stage in which the drug fraction deeply embedded within the PCL structure underwent a longer diffusion path before release (Pohlmann et al., 2013).

In vitro results showed good biocompatibility of our PCL NPs in mouse and human tumor cell assays supporting previous data obtained in neuroblastoma (SH-SY5Y cells), prostate cancer (PC3, DU-145 and LNCaP cells), lung (A549 cells) and breast (MCF-7 cells) cancer, and even embryonic kidney cells (HEK-293) (Arunraj et al., 2013; Cheng et al., 2012; Guo et al., 2015; Li et al., 2013; Sanna et al., 2015). In addition, no PCL NPs showed toxicity when tested in the non-tumor cell line H9C2.

Interestingly, the use of PCL NPs to load DOX (DOX-loaded PCL NPs) produced a significant increase in the drug's antitumoral activity against all the cell lines tested compared to free DOX, reducing the DOX IC50 value reducing the DOX IC50 value between 2.3 and 2.75 fold for lung cancer and between 7.8 and 65 fold for breast cancer. By contrast, DOX-loaded PCL NPs did not increase DOX toxicity in the non-tumor cell line H9C2. Many authors have also reported an increment in the cytotoxic effects of several drugs in some cancers when carried by PCL NPs. In fact, celastrol-loaded PCL NPs increased drug activity by up to 40% against PC3 prostate carcinoma cells compared with free celastrol (Sanna et al., 2015), carboplatin was able to reduce IC50 up to 3.06 times in the glioblastoma-astrocytoma cell line U-87 MG when was carried by PCL NPs (Karanam et al., 2015) and some triblock copolymers that included PCL improved the anti-tumor activity of DOX in the B16F10 melanoma cells (Shi et al., 2014). Recently, Suksiriworapong et al. (2016) have showed a significant decrease in quercetin IC_{50} (up to 4.6) using quercetin-loaded copolymers of PCL-co-d-a-tocopheryl PEG 1000 succinate in the SK-BR-3 breast cancer cell line. Concretely, DOX-loaded PCL NPs improved the activity of DOX in lung and breast cancer in comparison to other nanoformulations. In fact, we showed a higher decrease in A-549 proliferation with PCL-DOX NPs than the one described by Arunraj et al. (2013) using DOX-loaded chitin-PCL composite nanogels. This NPs showed an IC_{50} 1.6 fold higher than DOX, despite of their good cellular internalization. Mesoporous silica NPs loaded with DOX induced a smaller IC_{50} decrease than DOX-loaded PCL NPs in the same breast cancer cell line (MCF-7) (Gao et al., 2011). Furthermore, DOX-loaded PCL NPs induced higher cytotoxicity than calcium phosphate-reinforced polymer (Min et al., 2012) or Smac peptide-conjugated NPs (Li et al., 2015) in breast cancer cells. For example, the DOX IC_{50} decrease demonstrated by Li et al. (2015) in the MDA-MB-231 breast cancer cells (2.22 fold) was lower than the one induced by PCL-DOX NPs in MCF-7 and E0071 breast cancer cells (7.8 fold and 65 fold respectively). Recently, Eatemadi et al. (2016) also showed a DOX IC_{50} decrease using DOX-loaded PCL-polyethylene glycol NPs in both T47D (1.84 fold) and MCF7 (1.85 fold) breast cancer cell lines.

The transport of drugs, including DOX, towards the tumor cell may be facilitated by PCL NPs, resulting in increased antitumoral activity (Zheng et al., 2011). Karanam et al. (2015) showed a significant increase in the presence of the fluorochrome fluorescein isothiocyanate (FITC) in the U-87 MG cells when it was carried by PCL NPs (1 and 4 h of exposure). Fluorescence microscopy and FACScan analysis demonstrated that DOX-loaded PCL NPs penetrated efficiently into breast and lung cancer cells with a significant increase of drug uptake by the cell through time in comparison to free DOX. Recently, Suksiriworapong et al. (2016) showed that coumarin-6-loaded P (CL)-TPGS NPs were also able to increase NP cell uptake in SK-BR-3 cells through time (1, 2 and 4 h). The greater antiproliferative effect of DOX-loaded NPs compared to free drug could be related to an increased cell uptake in tumor cells, due their endocytic pathway deregulation (Mellman and Yarden, 2013; Elkin et al., 2015). This fact could be the reason for the non-enhanced toxicity of DOX-loaded PCL NPs in the non-tumor H9C2 cells. Interestingly, although the intracellular localization of DOX (nucleus/cytoplasm) was similar after treatments with DOX-loaded NPs and free DOX, a greater presence of DOX in cytoplasm was detected with the use of the PCL NPs. These results support studies showing a higher cytoplasmic location of DOX when loaded in PCL NPs in comparison to free DOX, possibly due to the continuous release of DOX from the polymer (Cheng et al., 2012; Li et al., 2013). Other studies showed a cytoplasmic localization of the FITC-loaded copolymer using copolymers of PEG-PCL-polyethylenimine (PCIF) loaded with DOX and FITC in the 4T1 mouse breast cancer cell line while the intracellular location of DOX was predominantly nuclear (Guo et al., 2015). Recently, a preferential cytoplasmic localization around the nucleus was also observed with the use of coumarin-6-loaded PCL-PGS NPs (Suksiriworapong et al., 2016).

When DOX-loaded PCL NPs were administered to mice bearing subcutaneous tumors of breast and lung cancer, a significant volume reduction (≈36%) in both tumors was demonstrated in comparison to those treated with free DOX (Fig. 6A). This increased antitumoral activity of the drug was accompanied by a clear increase in the survival rate, but only in the case of mice bearing lung tumors. There are not many *in vivo* studies with similar PCL NPs, but Wang et al. (2013) showed more limited results using curcumin and DOX cotransported in the micelles of PEG-PCL NPs in C57BL/6 mice bearing subcutaneous tumors from the LL/2 cell line in comparison to the free drug. Similar tumor volume progression was observed with some DOX-loaded polymer-caged nanobins or DOX-loaded non-mineralized micelles in lung or breast cancer xenograft models induced with MDA-MB-231 cells (Lee et al., 2010; Min et al., 2012). Recently, lipidic nanoformulations, such as nanostructured lipid carriers and liposomes, also improved the DOX antitumor activity in a breast cancer *in vivo* model induced by the 4T1 cell line (Fernandes et al., 2016). However, unlike DOX-loaded PCL NPs, none of these latter nanoformulations were assayed for cardiotoxicity or hematological toxicity.

In addition, PCL NPs may be improved by using magnetic nanoparticles, as recently shown by Tang et al. (2016) who obtained an increased DOX accumulation around the tumor tissues (murine hepatocarcinoma from the H22 cell line) using magnetic PCL-PEG micelles. Other drugs such as quercetin and genistein have shown improved *in vivo* antitumor activity thanks to the use of PCL NPs. Quercetin-loaded monomethoxy PEG-PCL and genistein-loaded TPGS-*b*-PCL NPs induced a greater reduction in the tumor volume of BALB/c mice bearing colon tumors from the CT26 and HeLa cell lines, respectively (Xu et al., 2015; Zhang et al., 2015). The treatment was well tolerated, not inducing major alterations in the weight of the mice.

Finally, the modulation of DOX toxicity through association with PCL NPs was analyzed in the mice. Administering a single dose of free DOX (10 mg of DOX/kg body weight) induced some myocardium injury, supported by a significant increase in the CRP cardiovascular damage marker in serum. In addition, free DOX altered blood parameters in mice, inducing a significant decrease in the WBC value. Interestingly, the DOX-loaded PCL NP treatment neither modified the WBC value nor altered the tissue histology or cardiovascular damage blood markers (MMP-9, sVACM-1 and CRP) compared to the control mice. These blood markers are currently used to detect cardiovascular diseases (Chua et al., 2016; Ky et al., 2014; Okur et al., 2016) and it is known that they increase in blood when DOX is administered, particularly in the case of CRP (Ky et al., 2014). These results therefore suggest that DOX-loaded PCL NPs reduce the classical drug toxicity in myocardium, as well as blood toxicity. In fact, modulation of the DOX biodistribution caused by the use of a nanocarrier (PCL NP) may be correlated with changes in the accumulation of DOX in cardiac tissue (Chen et al., 2013, 2016; Tran et al., 2014; Xie et al., 2014). Neither free DOX nor DOX-loaded PCL NP treatments caused weight loss or other alterations in tissues, such as the lungs (pulmonary congestion) or liver (hepatocytes necrosis), probably due to the DOX dosage administered (Zhu et al., 2014). In this context, decreased DOX toxicity with the use of PCL NPs as the carrier, has also been recently described by Sun et al. (2016), demonstrating less modulation of the WBC and MPV blood parameters in mice with melanoma with the use monomethoxy PEG-PCL-DOX NPs in comparison to the free drug. Similar results were reported by Chen et al. (2016) when DOX and PTX-loaded PCL NPs were used to co-treat BALB/c nude mice bearing subcutaneous KBv tumors.

5. Conclusion

In conclusion, the *in vitro* analysis of DOX-loaded PCL NPs demonstrated a significant increase of DOX cytotoxicity in all lung and breast cancer cells tested, in comparison to free DOX, causing a decrease of up to 98% of the drug IC50 (E0771 cell line). Biodegradable PCL nanocarriers showed good biocompatibility even at the highest concentrations. In addition, DOX-loaded PCL NPs increased drug internalization in both breast and lung tumor cells. An analysis of breast and lung cancer xenografts showed a greater reduction in tumor volume (up to 36%) when DOX-loaded PCL NPs were used in comparison to free DOX. Moreover, DOX-loaded PCL NPs were able to reduce DOX toxicity *in vivo* without causing myocardial injury or modulation of blood cell parameters. The results with the DOX-loaded PCL NP formulation suggest that it has significant potential for further translation into clinical applications.

Supplementary data to this article can be found online at http://dx.doi.org/10.1016/j.ejps.2017.02.026.

Acknowledgements

Research leading to these results has received funding by the Consejería de Salud from Junta de Andalucía (Spain) through projects Project PI-0476-2016 and P11-CTS-7649 and by University of Granada project PP2015-13. The authors wish to express their gratitude to G. Ortiz Ferron (CIC, University of Granada, Spain) for his skillful assistance with cytometry experiments. All authors have given approval to the final version of the manuscript.

References

Angsutararux, P., Luanpitpong, S., Issaragrisil, S., 2015. Chemotherapy-induced cardiotoxicity: overview of the roles of oxidative stress. Oxidative Med. Cell. Longev. 2015:795602. http://dx.doi.org/10.1155/2015/795602.

Arias, J.L., López-Viota, M., Sáez-Fernández, E., Ruiz, M.A., 2010. Formulation and physicochemical characterization of poly(epsilon-caprolactone) nanoparticles loaded with ftorafur and diclofenac sodium. Colloids Surf. B Biointerfaces 75:204–208. http://dx.doi.org/10.1016/j.colsurfb.2009.08.032.

Arunraj, T.R., Sanoj Rejinold, N., Ashwin Kumar, N., Jayakumar, R., 2013. Doxorubicin-chitin-poly(caprolactone) composite nanogel for drug delivery. Int. J. Biol. Macromol. 62:35–43. http://dx.doi.org/10.1016/j.ijbiomac.2013.08.013.

Blanco, E., Ferrari, M., 2014. Emerging nanotherapeutic strategies in breast cancer. Breast (Edinb. Scotl.) 23:10–18. http://dx.doi.org/10.1016/j.breast.2013.10.006.

Chen, Y., Yang, W., Chang, B., Hu, H., Fang, X., Sha, X., 2013. In vivo distribution and antitumor activity of doxorubicin-loaded *N*-isopropylacrylamide-co-methacrylic acid coated mesoporous silica nanoparticles and safety evaluation. Eur. J. Pharm. Biopharm. 85:406–412. http://dx.doi.org/10.1016/j.ejpb.2013.06.015.

Chen, Y., Zhang, W., Huang, Y., Gao, F., Fang, X., 2016. In vivo biodistribution and antitumor efficacy evaluation of doxorubicin and paclitaxel-loaded pluronic micelles decorated with c(RGDyK) peptide. PLoS One 11, e0149952. http://dx.doi.org/10.1371/journal.pone.0149952.

Cheng, Y., Hao, J., Lee, L.A., Biewer, M.C., Wang, Q., Stefan, M.C., 2012. Thermally controlled release of anticancer drug from self-assembled γ-substituted amphiphilic poly(ε-caprolactone) micellar nanoparticles. Biomacromolecules 13:2163–2173. http://dx.doi.org/10.1021/bm300823y.

Chua, S., Lee, F.-Y., Chiang, H.-J., Chen, K.-H., Lu, H.-I., Chen, Y.-T., Yang, C.-C., Lin, K.-C., Chen, Y.-L., Kao, G.-S., Chen, C.-H., Chang, H.-W., Yip, H.-K., 2016. The cardioprotective effect of melatonin and exendin-4 treatment in a rat model of cardiorenal syndrome. J. Pineal Res. 61:438–456. http://dx.doi.org/10.1111/jpi.12357.

Cirpanli, Y., Allard, E., Passirani, C., Bilensoy, E., Lemaire, L., Calış, S., Benoit, J.-P., 2011. Antitumoral activity of camptothecin-loaded nanoparticles in 9L rat glioma model. Int. J. Pharm. 403:201–206. http://dx.doi.org/10.1016/j.ijpharm.2010.10.015.

Dash, T.K., Konkimalla, V.B., 2012. Poly-ε-caprolactone based formulations for drug delivery and tissue engineering: a review. J. Control. Release 158:15–33. http://dx.doi.org/10.1016/j.jconrel.2011.09.064.

Decuzzi, P., Pasqualini, R., Arap, W., Ferrari, M., 2009. Intravascular delivery of particulate systems: does geometry really matter? Pharm. Res. 26:235–243. http://dx.doi.org/10.1007/s11095-008-9697-x.

Doroshow, J.H., 1983. Effect of anthracycline antibiotics on oxygen radical formation in rat heart. Cancer Res. 43, 460–472.

Eatemadi, A., Darabi, M., Afraidooni, L., Zarghami, N., Daraee, H., Eskandari, L., Mellatyar, H., Akbarzadeh, A., 2016. Comparison, synthesis and evaluation of anticancer drug-loaded polymeric nanoparticles on breast cancer cell lines. Artif. Cells Nanomed. Biotechnol. 44:1008–1017. http://dx.doi.org/10.3109/21691401.2015.100851.

Elkin, S.R., Bendris, N., Reis, C.R., Zhou, Y., Xie, Y., Huffman, K.E., Minna, J.D., Schmid, S.L., 2015. A systematic analysis reveals heterogeneous changes in the endocytic activities of cancer cells. Cancer Res. 75:4640–4650. http://dx.doi.org/10.1158/0008–5472.

Ferlay, J., Soerjomataram, I., Ervik, M., Dikshit, R., Eser, S., Mathers, C., Rebelo, M., Parkin, D.M., Forman, D., Bray, F., 2013. GLOBOCAN 2012 v1.0, Cancer Incidence and Mortality Worldwide: IARC CancerBase No. 11. International Agency for Research on Cancer, Lyon, France http://globocan.iarc.fr (accessed on day/month/year accessed 11.11.15).

Fernandes, R.S., Silva, J.O., Monteiro, L.O., Leite, E.A., Cassali, G.D., Rubello, D., Cardoso, V.N., Ferreira, L.A., Oliveira, M.C., de Barros, A.L., 2016. Doxorubicin-loaded nanocarriers: a comparative study of liposome and nanostructured lipid carrier as alternatives for cancer therapy. Biomed. Pharmacother. 84:252–257. http://dx.doi.org/10.1016/j.biopha.2016.09.032.

Gao, Y., Chen, Y., Ji, X., He, X., Yin, Q., Zhang, Z., Shi, J., Li, Y., 2011. Controlled intracellular release of doxorubicin in multidrug-resistant cancer cells by tuning the shell-pore sizes of mesoporous silica nanoparticles. ACS Nano 5:9788–9798. http://dx.doi.org/10.1021/nn2033105.

Gou, M., Zheng, X., Men, K., Zhang, J., Zheng, L., Wang, X., Luo, F., Zhao, Y., Zhao, X., Wei, Y., Qian, Z., 2009. Poly(epsilon-caprolactone)/poly(ethylene glycol)/poly(epsilon-caprolactone) nanoparticles: preparation, characterization, and application in doxorubicin delivery. J. Phys. Chem. B 113:12928–12933. http://dx.doi.org/10.1021/jp905781g.

Gou, M., Wei, X., Men, K., Wang, B., Luo, F., Zhao, X., Wei, Y., Qian, Z., 2011. PCL/PEG copolymeric nanoparticles: potential nanoplatforms for anticancer agent delivery. Curr. Drug Targets 12, 1131–1150.

Govender, J., Loos, B., Marais, E., Engelbrecht, A.-M., 2014. Mitochondrial catastrophe during doxorubicin-induced cardiotoxicity: a review of the protective role of melatonin. J. Pineal Res. 57:367–380. http://dx.doi.org/10.1111/jpi.12176.

Guo, Q., Kuang, L., Cao, H., Li, W., Wei, J., 2015. Self-assembled mPEG-PCL-g-PEI micelles for multifunctional nanoprobes of doxorubicin delivery and magnetic resonance imaging and optical imaging. Colloids Surf. B Biointerfaces 136:687–693. http://dx.doi.org/10.1016/j.colsurfb.2015.10.013.

Hira, S.K., Mishra, A.K., Ray, B., Manna, P.P., 2014. Targeted delivery of doxorubicin-loaded poly (ε-caprolactone)-*b*-poly (*N*-vinylpyrrolidone) micelles enhances antitumor effect in lymphoma. PLoS One 9, e94309. http://dx.doi.org/10.1371/journal.pone.0094309.

Karanam, V., Marslin, G., Krishnamoorthy, B., Chellan, V., Siram, K., Natarajan, T., Bhaskar, B., Franklin, G., 2015. Poly (ε-caprolactone) nanoparticles of carboplatin: preparation, characterization and in vitro cytotoxicity evaluation in U-87 MG cell lines. Colloids Surf. B Biointerfaces 130:48–52. http://dx.doi.org/10.1016/j.colsurfb.2015.04.005.

Kumar, A., Lale, S.V., Mahajan, S., Choudhary, V., Koul, V., 2015. ROP and ATRP fabricated dual targeted redox sensitive polymersomes based on pPEGMA-PCL-ss-PCL-pPEGMA triblock copolymers for breast cancer therapeutics. ACS Appl. Mater. Interfaces 7:9211–9227. http://dx.doi.org/10.1021/acsami.5b01731.

Ky, B., Putt, M., Sawaya, H., French, B., Januzzi, J.L., Sebag, I.A., Plana, J.C., Cohen, V., Banchs, J., Carver, J.R., Wiegers, S.E., Martin, R.P., Picard, M.H., Gerszten, R.E., Halpern, E.F., Passeri, J., Kuter, I., Scherrer-Crosbie, M., 2014. Early increases in multiple biomarkers predict subsequent cardiotoxicity in patients with breast cancer treated with doxorubicin, taxanes, and trastuzumab. J. Am. Coll. Cardiol. 63:809–816. http://dx.doi.org/10.1016/j.jacc.2013.10.061.

Lee, S.M., Ahn, R.W., Chen, F., Fought, A.J., O'Halloran, T.V., Cryns, V.L., Nguyen, S.T., 2010. Biological evaluation of pH-responsive polymer-caged nanobins for breast cancer therapy. ACS Nano 4:4971–4978. http://dx.doi.org/10.1021/nn100560p.

Lee, R.-S., Li, Y.-C., Wang, S.-W., 2015. Synthesis and characterization of amphiphilic photocleavable polymers based on dextran and substituted-ε-caprolactone. Carbohydr. Polym. 117:201–210. http://dx.doi.org/10.1016/j.carbpol.2014.09.062.

Letchford, K., Liggins, R., Wasan, K.M., Burt, H., 2009. In vitro human plasma distribution of nanoparticulate paclitaxel is dependent on the physicochemical properties of poly(-ethylene glycol)-*block*-poly(caprolactone) nanoparticles. Eur. J. Pharm. Biopharm. 71:196–206. http://dx.doi.org/10.1016/j.ejpb.2008.08.003.

Li, B., Wang, Q., Wang, X., Wang, C., Jiang, X., 2013. Preparation, drug release and cellular uptake of doxorubicin-loaded dextran-*b*-poly(ε-caprolactone) nanoparticles. Carbohydr. Polym. 93:430–437. http://dx.doi.org/10.1016/j.carbpol.2012.12.051.

Li, M., Liu, P., Gao, G., Deng, J., Pan, Z., Wu, X., Xie, G., Yue, C., Cho, C.H., Ma, Y., Cai, L., 2015. Smac therapeutic peptide nanoparticles inducing apoptosis of cancer cells for combination chemotherapy with doxorubicin. ACS Appl. Mater. Interfaces 7:8005–8012. http://dx.doi.org/10.1021/acsami.5b00329.

Liu, Q., Li, R.-T., Qian, H.-Q., Yang, M., Zhu, Z.-S., Wu, W., Qian, X.-P., Yu, L.-X., Jiang, X.-Q., Liu, B.-R., 2012. Gelatinase-stimuli strategy enhances the tumor delivery and therapeutic efficacy of docetaxel-loaded poly(ethylene glycol)-poly(ε-caprolactone) nanoparticles. Int. J. Nanomedicine 7:281–295. http://dx.doi.org/10.2147/IJN.S26697.

Marslin, G., Sarmento, B.F.C.C., Franklin, G., Martins, J.A.R., Silva, C.J.R., Gomes, A.F.C., Sárria, M.P., Coutinho, O.M.F.P., Dias, A.C.P., 2016. Curcumin encapsulated into methoxy poly(ethylene glycol) poly(ε-caprolactone) nanoparticles increases cellular uptake and neuroprotective effect in glioma cells. Planta Med. http://dx.doi.org/10.1055/s-0042-112030.

Melguizo, C., Cabeza, L., Prados, J., Ortiz, R., Caba, O., Rama, A.R., Delgado, Á.V., Arias, J.L., 2015. Enhanced antitumoral activity of doxorubicin against lung cancer cells using biodegradable poly(butylcyanoacrylate) nanoparticles. Drug Des. Devel. Ther. 9: 6433–6444. http://dx.doi.org/10.2147/DDDT.S92273.

Mellman, I., Yarden, Y., 2013. Endocytosis and cancer. Cold Spring Harb. Perspect. Biol. 5: a016949. http://dx.doi.org/10.1101/cshperspect.a016949.

Min, K.H., Lee, H.J., Kim, K., Kwon, I.C., Jeong, S.Y., Lee, S.C., 2012. The tumor accumulation and therapeutic efficacy of doxorubicin carried in calcium phosphate-reinforced polymer nanoparticles. Biomaterials 33:5788–5797. http://dx.doi.org/10.1016/j.biomaterials.2012.04.057.

Okur, A., Karadeniz, C., Özhan Oktar, S., Pınarlı, F.G., Aral, A., Oğuz, A., 2016. Assessment of brachial artery reactivity, carotid intima-media thickness, and adhesion molecules in pediatric solid tumor patients treated with anthracyclines. Pediatr. Hematol. Oncol. 33:178–185. http://dx.doi.org/10.3109/08880018.2016.1146375.

Ortiz, R., Cabeza, L., Arias, J.L., Melguizo, C., Álvarez, P.J., Vélez, C., Clares, B., Áranega, A., Prados, J., 2015. Poly(butylcyanoacrylate) and poly(ε-caprolactone) nanoparticles loaded with 5-fluorouracil increase the cytotoxic effect of the drug in experimental colon cancer. AAPS J. 17:918–929. http://dx.doi.org/10.1208/s12248-015-9761-5.

Pohlmann, A.R., Fonseca, F.N., Paese, K., Detoni, C.B., Coradini, K., Beck, R.C., Guterres, S.S., 2013. Poly(ε-caprolactone) microcapsules and nanocapsules in drug delivery. Expert Opin. Drug Deliv. 10:623–638. http://dx.doi.org/10.1517/17425247.2013.769956.

Sanna, V., Chamcheu, J.C., Pala, N., Mukhtar, H., Sechi, M., Siddiqui, I.A., 2015. Nanoencapsulation of natural triterpenoid celastrol for prostate cancer treatment. Int. J. Nanomedicine 10:6835–6846. http://dx.doi.org/10.2147/IJN.S93752.

Shi, S., Shi, K., Tan, L., Qu, Y., Shen, G., Chu, B., Zhang, S., Su, X., Li, X., Wei, Y., Qian, Z., 2014. The use of cationic MPEG-PCL-g-PEI micelles for co-delivery of Msurvivin T34A gene and doxorubicin. Biomaterials 35:4536–4547. http://dx.doi.org/10.1016/j.biomaterials.2014.02.010.

Suksiriworapong, J., Phoca, K., Ngamsom, S., Sripha, K., Moongkarndi, P., Junyaprasert, V.B., 2016. Comparison of poly(ε-caprolactone) chain lengths of poly(ε-caprolactone)-*co*-*d*-α-tocopheryl-poly(ethylene glycol) 1000 succinate nanoparticles for enhancement of quercetin delivery to SKBR3 breast cancer cells. Eur. J. Pharm. Biopharm. 101:15–24. http://dx.doi.org/10.1016/j.ejpb.2016.01.008.

Sun, C., Zhou, L., Gou, M., Shi, S., Li, T., Lang, J., 2016. Improved antitumor activity and reduced myocardial toxicity of doxorubicin encapsulated in MPEG-PCL nanoparticles. Oncol. Rep. 35:3600–3606. http://dx.doi.org/10.3892/or.2016.4748.

Tacar, O., Sriamornsak, P., Dass, C.R., 2013. Doxorubicin: an update on anticancer molecular action, toxicity and novel drug delivery systems. J. Pharm. Pharmacol. 65: 157–170. http://dx.doi.org/10.1111/j.2042-7158.2012.01567.x.

Tang, Z., Zhang, L., Wang, Y., Li, D., Zhong, Z., Zhou, S., 2016. Redox-responsive star-shaped magnetic micelles with active-targeted and magnetic-guided functions for cancer therapy. Acta Biomater. 42:232–246. http://dx.doi.org/10.1016/j.actbio.2016.06.038.

Tran, T.-H., Nguyen, C.T., Gonzalez-Fajardo, L., Hargrove, D., Song, D., Deshmukh, P., Mahajan, L., Ndaya, D., Lai, L., Kasi, R.M., Lu, X., 2014. Long circulating self-assembled nanoparticles from cholesterol-containing brush-like block copolymers for improved drug delivery to tumors. Biomacromolecules 15:4363–4375. http://dx.doi.org/10.1021/bm5013822.

Vejpongsa, P., Yeh, E.T.H., 2014. Topoisomerase 2β: a promising molecular target for primary prevention of anthracycline-induced cardiotoxicity. Clin. Pharmacol. Ther. 95: 45–52. http://dx.doi.org/10.1038/clpt.2013.201.

Wang, B.-L., Shen, Y., Zhang, Q., Li, Y., Luo, M., Liu, Z., Li, Y., Qian, Z., Gao, X., Shi, H., 2013. Codelivery of curcumin and doxorubicin by MPEG-PCL results in improved efficacy of systemically administered chemotherapy in mice with lung cancer. Int. J. Nanomedicine 8:3521–3531. http://dx.doi.org/10.2147/IJN.S45250.

Wei, X., Gong, C., Gou, M., Fu, S., Guo, Q., Shi, S., Luo, F., Guo, G., Qiu, L., Qian, Z., 2009. Biodegradable poly(epsilon-caprolactone)-poly(ethylene glycol) copolymers as drug delivery system. Int. J. Pharm. 381:1–18. http://dx.doi.org/10.1016/j.ijpharm.2009.07.033.

Weiss, R.B., 1992. The anthracyclines: will we ever find a better doxorubicin? Semin. Oncol. 19, 670–686.

Xie, M., Xu, Y., Shen, H., Shen, S., Ge, Y., Xie, J., 2014. Negative-charge-functionalized mesoporous silica nanoparticles as drug vehicles targeting hepatocellular carcinoma. Int. J. Pharm. 474:223–231. http://dx.doi.org/10.1016/j.ijpharm.2014.08.027.

Xu, G., Shi, H., Ren, L., Gou, H., Gong, D., Gao, X., Huang, N., 2015. Enhancing the anti-colon cancer activity of quercetin by self-assembled micelles. Int. J. Nanomedicine 10: 2051–2063. http://dx.doi.org/10.2147/IJN.S75550.

Zhang, J., Men, K., Gu, Y., Wang, X., Gou, M., Guo, G., Luo, F., Qian, Z., 2011. Preparation of core cross-linked PCL-PEG-PCL micelles for doxorubicin delivery in vitro. J. Nanosci. Nanotechnol. 11, 5054–5061.

Zhang, H., Liu, G., Zeng, X., Wu, Y., Yang, C., Mei, L., Wang, Z., Huang, L., 2015. Fabrication of genistein-loaded biodegradable TPGS-*b*-PCL nanoparticles for improved therapeutic effects in cervical cancer cells. Int. J. Nanomedicine 10:2461–2473. http://dx.doi.org/10.2147/IJN.S78988.

Zheng, L., Gou, M., Zhou, S., Yi, T., Zhong, Q., Li, Z., He, X., Chen, X., Zhou, L., Wei, Y., Qian, Z., Zhao, X., 2011. Antitumor activity of monomethoxy poly(ethylene glycol)-poly (ε-caprolactone) micelle-encapsulated doxorubicin against mouse melanoma. Oncol. Rep. 25:1557–1564. http://dx.doi.org/10.3892/or.2011.1243.

Zhu, Q., Jia, L., Gao, Z., Wang, C., Jiang, H., Zhang, J., Dong, L., 2014. A tumor environment responsive doxorubicin-loaded nanoparticle for targeted cancer therapy. Mol. Pharm. 11:3269–3278. http://dx.doi.org/10.1021/mp4007776.

Zhu, Y., Sun, Y., Chen, Y., Liu, W., Jiang, J., Guan, W., Zhang, Z., Duan, Y., 2015. In vivo molecular MRI imaging of prostate cancer by targeting PSMA with polypeptide-labeled superparamagnetic iron oxide nanoparticles. Int. J. Mol. Sci. 16:9573–9587. http://dx.doi.org/10.3390/ijms16059573.